

Multiphoton absorption excited upconversion luminescence in optical fiber

Fabio Mangini,^{1,*} Mario Ferraro,^{2,*} Mario Zitelli,² Alioune Niang,¹
Alessandro Tonello,³ Vincent Couderc,³ and Stefan Wabnitz^{2,4}

¹*Department of Information Engineering, University of Brescia, Via Branze 38, 25123 Brescia, Italy.*

²*Department of Information Engineering, Electronics, and Telecommunications,
Sapienza University of Rome, Via Eudossiana 18, 00184 Rome, Italy*

³*Université de Limoges, XLIM, UMR CNRS 7252,
123 Avenue A. Thomas, 87060 Limoges, France*

⁴*Novosibirsk State University, Pirogova 1, Novosibirsk 630090, Russia*

(Dated: December 5, 2020)

We experimentally demonstrate a **previously unforeseen** nonlinear effect in optical fibers: upconversion luminescence generation excited by multiphoton absorption of femtosecond infrared pulses. We directly estimate the average number of photons involved in the up-conversion process, by varying the wavelength of the pump source. We highlight the role of non-bridging oxygen hole centers and oxygen deficient center defects, and directly compare the intensity of side-scattered luminescence with numerical simulations of pulse propagation.

I. INTRODUCTION

Upconversion luminescence (UL), involving the absorption of multiple photons followed by the emission of higher energy photons via the radiative decay of excited electron energy levels in dielectric materials, has attracted considerable research attention, since its first observation in rare-earth-doped crystals [1]. Over the years, UL found application in a wide range of fields, moving from physics to chemistry and biology, since it allows for the detection of several stimuli such as temperature, electromagnetic radiation and pH [2]. Thanks to materials nanoengineering development, UL has been recently proposed for medical therapy too [3]. In physics, UL finds its main application in the generation of visible laser emission by means of infrared optical pumping [4, 5].

Aiming to the realization of fiber lasers, various authors have studied UL in optical fibers, doped with different types of semiconductors, such as cesium, europium, and tantalum [6–8]. In their first report of UL in silica glass, which is the main constituent of commercial optical fibers, Kazansky et al. attributed their observation of multiphoton absorption (MPA) excited upconversion luminescence in Ge-doped silica glass to the presence of Germanium Oxygen deficient center (Ge-ODC) defects [9]. However, intrinsic and induced defects in silica were already studied by using ultraviolet (UV)-pumped visible photoluminescence. Among these, the presence of the so-called non-bridging Oxygen hole center (NBOHC) defects, responsible for visible red light emission at 650 nm, attracted significant interest [10]. NBOHCs consist of a complementary pair of broken silicon-oxygen bonds, and were among the first defects to be studied. Their paramagnetic properties permit to investigate NBOHCs

by means of the electron paramagnetic resonance technique. Only later, the presence of diamagnetic defects, such as Ge-OCDCs, was also discovered in silica glass [11]. These defects are responsible for several luminescence bands in the UV-VIS spectral range. Three main emission bands, centered at 290, 400 and 460 nm, were easily detected in as-grown or irradiated silica [12, 13], as well as in Ge-doped silica [14]. Ge-ODC luminescence was also observed in singlemode optical fibers [15], and it was proposed as an alignment marker for the manufacturing of fiber Bragg gratings [16]. Luminescence from defects and impurities represents a useful tool for the spectroscopy of transparent media, and permits to extend the range of laser emission into the UV. Luminescence was recently proposed as a tool for supercontinuum generation in YAG crystals [17]. In optical fibers, UL provides an interesting means to extend the supercontinuum bandwidth into the UV, which is otherwise challenging by using parametric nonlinear effects [18, 19].

In this Letter, we report the experimental observation and theoretical description of visible UL in commercial multimode fibers (MMFs), pumped by intense femtosecond infrared laser pulses. Owing to their large numerical aperture, MMFs are better suited than singlemode fibers to trap luminescent radiation. Moreover, because of their relatively large core size, MMFs may carry light beams with peak powers up to the self-focusing critical value, before any permanent damage occurs. This allows for the observation of a host of **unexpected** nonlinear effects [18, 20]. Specifically, the presence of photoluminescence and nonlinear losses, which were ascribed to a MPA mechanism, was recently reported in graded-index (GRIN) MMFs [21, 22]. These nonlinear losses introduce a fundamental, and previously undisclosed, nonlinear limitation to the energy transmission capabilities of optical fibers, and may provide an intrinsic limitation for the power scaling of spatiotemporal mode-locking with multimode fiber lasers [23].

To date, a microscopic interpretation of these intriguing phenomena is still missing. Here we fill this gap of

* These two authors contributed equally
mario.ferraro@uniroma1.it

knowledge, by associating them to UL. Specifically, we unveil a previously unforeseen nonlinear phenomenon in optical fibers, by demonstrating the presence of up to 5-photon absorption processes involved in UL generation. Spatial self-imaging (SSI) in GRIN fibers plays key role in enhancing UL, which becomes visible to the naked eye as an array of side-scattering blue emitters. Our experimental results are in excellent quantitative agreement with numerical simulations, based on a generalized nonlinear Schrödinger equation (GNLS). We provide a complete characterization of the multiphoton nature of UL, by varying the laser power and wavelength, and compare UL spectra for GRIN and step-index MMFs.

II. METHODS

In our experiments, we measured the spectrum of visible UL light scattered out of the first few millimeters of propagation in MMFs. This light results from the multiphoton absorption of high peak power (up to 3 MW) femtosecond infrared pulses. Spectra were collected with a miniature fiber optics spectrometer (Avaspec-2048). As a pump source, we used a hybrid optical parametric amplifier (OPA) pumped by a femtosecond Yb-based laser. Pulses of 80 fs at 650-940 nm and 180 fs at 1030 nm with 100 kHz repetition rate were coupled into two different multimode standard fibers: a 50/125 GRIN fiber with a relative index difference $\Delta_{GRIN} = 0.0103$, and a 105/125 step-index fiber with $\Delta_{SI} = 0.012$. In both cases, the beam ($1/e^2$) diameter at the fiber input facet was equal to $7.55 \mu\text{m}$ at $\lambda = 1030 \text{ nm}$, and about $11 \mu\text{m}$ at $\lambda = 650 - 940 \text{ nm}$. UL was collected by means of an imaging lens into either the spectrometer or a microscope.

In Fig.1a we present a sketch of our setup. Fig.1b shows pictures of the side-scattered UL spots, taken by a Dinolite-AM3113T digital microscope. The different scattering patterns from either GRIN or step-index fibers can be clearly appreciated. A single emission spot at the point of minimum beam waist is scattered from the step-index fiber. Whereas the periodic beam focusing in the GRIN fiber leads to an array of scattering points. The two fibers also differ in terms of their dopants and concentrations. Specifically, in the step-index fiber the cladding is made of fluorine-doped silica, while the core is nominally undoped. In contrast, index grading in the GRIN fiber is obtained by using a parabolically decreasing concentration of Ge dopant in the core, and the cladding is made of pure silica. In Fig.1c, a scanning electron microscope (SEM) image of the GRIN fiber facet is reported. We spatially tracked the Ge concentration along a diameter of the core (white line in the figure) by means of energy dispersive X-ray Spectroscopy (EDX), which provides a well-known signature in the electromagnetic spectrum. The result is shown in Fig.1d. At its peak, Ge-doping is 15 %-mass (corresponding to 4.5 %-atomic).

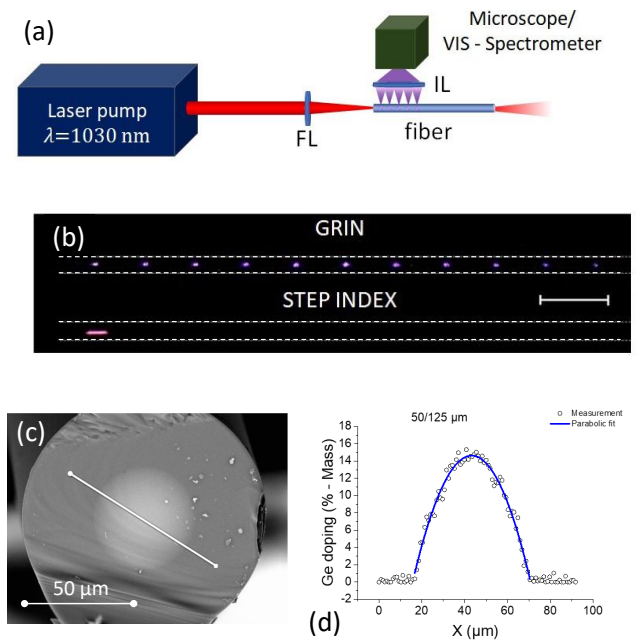


FIG. 1. (a) Schematic of the experimental setup. (b) Microscope image of luminescence scattered from either GRIN or step-index fibers. Dashed lines stand for the cladding-air interface, while the scale bar corresponds to 1 mm. (c) SEM image of a GRIN fiber section. (d) % mass Germanium concentration in the Ge-doped GRIN fiber.

III. RESULTS

In Fig.2a we illustrate the dependence of the measured spectrum of side-scattered light on the peak power (P_p) of the pump laser pulses at 1030 nm. As can be seen, a broad visible emission appears when P_p crosses a certain power threshold (around 1.5 MW). Beyond such power, one may distinguish the generation of three main spectral peaks at 650, 460, and 400 nm, respectively. Another peak at 345 nm is appreciable at the highest input powers. The latter, having a rather narrow bandwidth, can be easily identified with the third-harmonic of the pump laser. On the other hand, we may attribute the origin of the red peak at 650 nm to the presence of NBOHCs. Whereas the peaks at 460 and 400 nm can be ascribed to Ge-ODC. All of these peaks results from MPA of the pump source. We did not observe any luminescence peak at 240 nm, since it is negligible at room temperature [24].

A sketch of the MPA process involving $n = 5$ photons is shown in Fig.2b. Owing to MPA, an electron is excited into a higher energy band ($S_0 \rightarrow S_1$). Next, electron-phonon scattering allows the system to relax into an intermediate energy level, from which luminescence takes place, thus bringing back the electron to its ground state ($T_1 \rightarrow S_0$). The only constraint in this simple picture is that the number of photons involved must be large enough, in order to bring the electron to its upper level. One may also notice that a smaller number of photons

would be required for the $S_0 \rightarrow T_1$ transition. Nevertheless, the contribution of this transition to multiphoton absorption turns out to be negligible for NBOHC and Ge-ODC defects. Being theoretically forbidden because of symmetry reasons, its associated oscillation strength is, in fact, one million times smaller than the $S_0 \rightarrow S_1$ transition at room temperature [25]. Therefore, as a first approximation, we may only consider the presence of the n -photon absorption process. In this simplified model, the parameter n represents an effective number of photons involved in the MPA process, since it includes all the possible contributions that we are not explicitly taking into account. We may also assume that the upconversion rate is small enough, so that the following relationship holds between the UL intensity (I_{UL}) and the n -th power of P_p [26]:

$$I_{UL} = \alpha P_p^n, \quad (1)$$

where the parameter α includes the n -photon absorption cross-section, and the phase-matching condition between the laser pump and the luminescence radiation. In this sense, it worth noticing that the latter is isotropic, while the pump is mostly guided into the fiber core. Interestingly, the absorption bands corresponding to the NBOHCs and ODCs are quite close in energy. The first occurs at 258 nm, and the second at 241 nm [25]. Hence, UL generated by both defects is triggered by the same number of absorbed photons (specifically, $n = 5$ for a pump wave at $\lambda = 1030$ nm).

To confirm this, in Fig.2c, we illustrated the dependence of I_{UL} (calculated as the integral of the corresponding spectral peak as shown in Fig.2a) on P_p . Because of the overlap of the two ODC peaks at 400 and 460, we integrated them as if they were a single signal. Figure 2c shows that the two fitting curves in the $\log_{10} - \log_{10}$ plot are parallel lines with a slope equal to 5, thus confirming the prediction of the simple model of Eq.(1).

The estimation of the number of photons involved in the multi-photon absorption process allows us to properly model the intensity variation of UL along the propagation distance. The periodicity of the latter in GRIN fibers has already been pointed out as a result of the spatial-self imaging effect [18, 22, 27]. Nevertheless, the amplitude of the UL intensity variation along the propagation distance in a GRIN fiber could not be quantitatively reproduced.

In Figures 3a,b we report a microscope image of the UL scattered over the first centimeter of GRIN fiber, and its corresponding fluence variation with distance. This was obtained by a normalization of the image intensity for each pixel of propagation. The presence of slow oscillation of the amplitude of the UL peaks, whose first maximum occurs at about 3.5 mm, is highlighted by the solid line, which is drawn as a guide to the eye. Here the fiber length is limited to 10 mm: after that the metallic fiber holder introduces additional light scattering, which masks quantitative studies of the UL intensity. However, by employing longer samples, one notices a rapid quenching of visible light emission after the first few centimeters

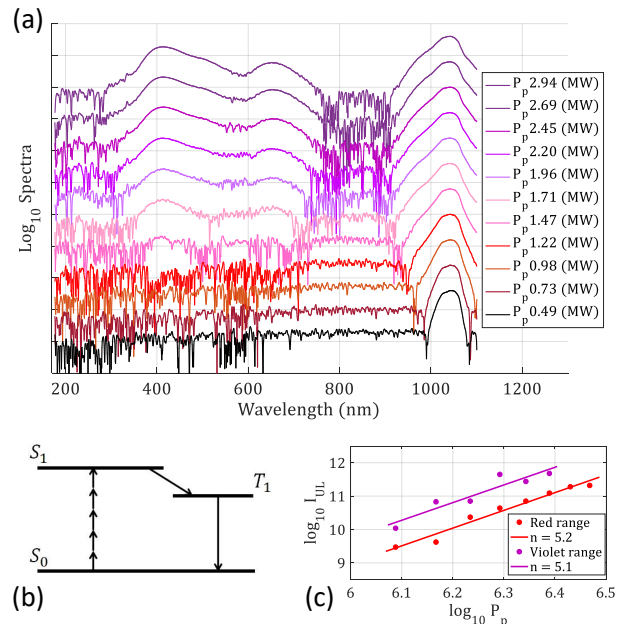


FIG. 2. (a) UL spectra in \log_{10} scale when varying the input peak power. (b) Sketch of a five-photon absorption UL mechanism. (c) $\log_{10} - \log_{10}$ plot of UL intensity as a function of input beam peak power. Experimental data (circles) are fitted by solid lines, whose slope n is written in the legend.

of fiber.

To further check the relation (1) between UL and MPA, we performed a numerical simulation of spatiotemporal beam propagation in the fiber. We used a scalar 3D+1 GNLS equation including second, third, and fourth-order dispersion, Kerr, and Raman nonlinearities, as described in Ref.[21]. Random phase noise was added to the input field, in order to describe the generation of intensity speckles, and seed the generation of supercontinuum and dispersive waves. Random changes in the fiber core diameter were also considered, although their effect is negligible here because of the short fiber length. Theoretically, in the case of $n = 5$ photon absorption, the UL fluence F_{UL} is related to the effective area A_{eff} and pulse duration Δt of the propagating laser beam by the formula:

$$F_{UL} \propto I^5 A_{eff} \Delta t = \frac{U^5}{A_{eff}^4 \Delta t^4}, \quad (2)$$

where I and U are the peak intensity and the energy of pulses along the fiber, respectively. Fig.3c shows that there is an excellent qualitative agreement between experiments and numerics in describing the variation of the UL emission along the fiber. In Fig.3d, our simulations highlight that the beam effective area A_{eff} rapidly oscillates with a constant amplitude along the propagation distance, because of SSI. Whereas the pulse duration Δt evolves over distances much longer than the SSI period. This means that the slow modulation of the UL emis-

sion in Fig.3a-c is due temporal pulse reshaping or broadening. In fact, the effective area is a time-independent quantity, calculated as:

$$A_{eff} = \frac{[\int dx dy (\int dt |E|(x, y, z, t))^2]^2}{\int dx dy (\int dt |E|(x, y, z, t))^4} \quad (3)$$

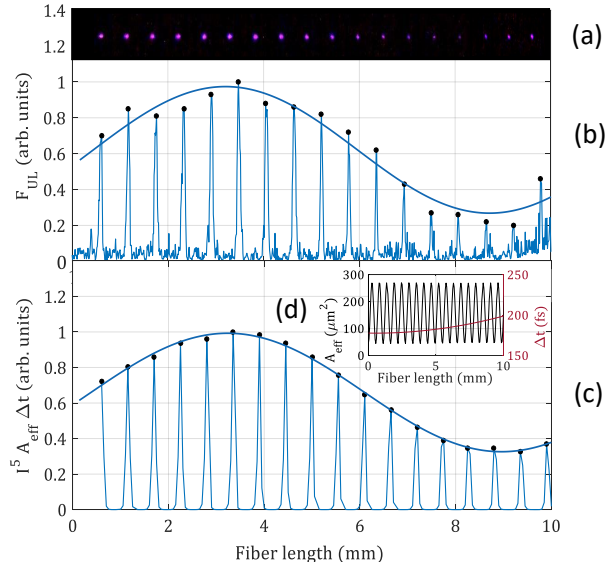


FIG. 3. (a) Digital microscope picture of light scattered from the GRIN fiber, showing periodic UL emission over the first centimeter. (b) 1D plot of the corresponding integrated normalized scattered intensity vs. propagation distance. The solid line is the envelope trend of the UL peaks (black dots) along with the fiber. (c) 1D plot of simulated UL fluence and its envelope. (d) Simulated beam effective area (black) and pulse duration (red) as function of the fiber length.

In order to further assess the validity of our model, we have varied the pump wavelength by using the OPA. In this way, the number of photons involved in the MPA process is also varied. We tuned the laser wavelength from 650 to 940 nm. In Fig.4a we illustrate the variation of the UL spectrum with pump laser wavelength, when the input peak power is kept constant at 2.2 MW. The Ge-ODC spectral peaks at 400 and 460 nm are present and clearly visible for pump wavelengths above 750 nm.

In Fig.4b we plot the Ge-ODC UL intensity as a function of the input peak power. We avoid referring to the NBOHC luminescence at 650 nm, since it is partially covered by the spectral broadening of the source. Again, the linear trend in the $\log_{10} - \log_{10}$ plots of Fig.4b allows us to estimate the average number of photons that are involved in the absorption, as reported in the legend. As can be seen, the average number of photons is reduced with respect to the previous case: here n ranges between 3.8 and 2.7 when the pump is swept from 940 to 750 nm. These

values are in agreement with predictions of our model. Indeed, we expected the number of photons to decrease down to $n = 3$ for $\lambda = 750$ nm, in order to match with the Ge-ODC absorption bands. Again, the discrepancy between theoretical and experimental values is rather small, in spite of our approximation that absorption is due to a single multiphoton process. The monotonic decrease of n as the laser wavelength is reduced clearly indicates the MPA nature of the observed UL.

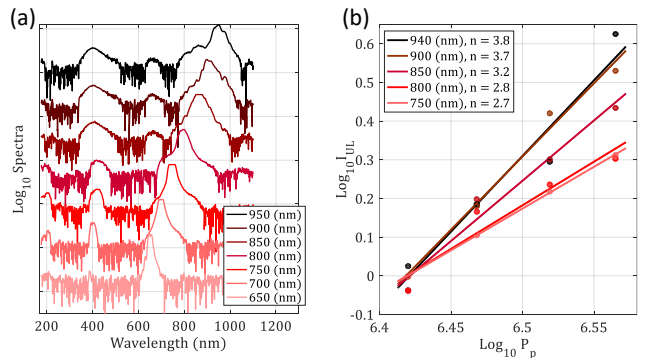


FIG. 4. (a) UL spectra in \log_{10} scale, when the pump wavelength varies between 650 and 940 nm. (b) $\log_{10} - \log_{10}$ plot of UL intensity vs. pump wavelength. Experimental data (circles) are fitted by solid lines, whose slope n appears in the legend.

For highlighting the effect of Ge-ODCs concentration on UL energy emission, we compared two GRIN fibers with different core diameters. These fibers also have different numerical apertures (NA), which grows larger with the Germanium doping concentration. In Fig.5 we show pictures of UL from either 0.2 or 0.275 NA GRIN fibers (with core diameters of 50 μm or 62.5 μm , respectively), under the same input coupling conditions. As it can be seen, UL from the larger NA fiber remains visible over a more than twice longer fiber length. Whereas the emitted UL energy is initially higher from the smaller effective area (or NA) fiber, because of the higher beam intensity in the emitting spots. Note that, because of the different core diameters, different SSI periods z_p result in the two fibers, according to the law [18] $z_p = \pi r_c / \sqrt{2\Delta}$, where r_c is the core radius and Δ is the core-cladding index difference. Because of the dependence of the SSI period on the core radius, by measuring the periodicity of UL emission one can use GRIN fibers as sensors, in order to reveal the presence of any kind of forces that may introduce a variation of the core size (e.g., mechanical or thermal stress).

We also compared UL emission of GRIN and step-index MMFs, see Fig.1b. A typical side-scattered spectrum obtained from a step-index fiber is reported as a black solid curve in Fig.6. For the ease of comparison, we also display as a green solid curve the UL spectrum obtained at the same power from a GRIN fiber, as in Fig.2a. Both spectra are normalized to the same intensity value

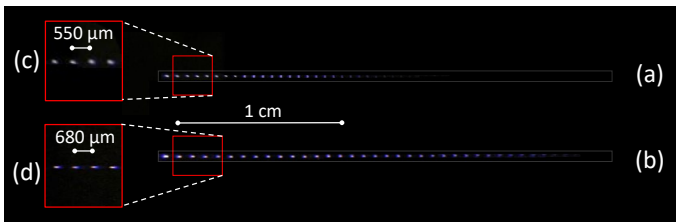


FIG. 5. (a) UL emission from a 50 μm core diameter GRIN fiber with NA = 0.2. (b) Same as (a), with NA = 0.275 and core diameter of 62.5 μm . (c) and (d) zoom-in of (a) and (b), respectively.

at 650 nm. In this way, we can appreciate that the contribution of NBOHCs is much lower in a step-index fiber, since its spectral component at 1030 nm is higher (here its peak value is cut by the saturation of the spectrometer) than that from the GRIN fiber. We can attribute this to the absence of spatial self-imaging, which increases the number of emitting spots and, as a consequence, the total contribution of NBOHC defects to scattered light. As far as the ODCs are concerned, the UL signal is much less intense in a step-index fiber than in a GRIN fiber. This can be attributed to the lack of extrinsic Ge atoms. Nevertheless, one can still easily recognize the presence of two peaks, which are slightly shifted with respect their respective positions for the GRIN fiber. We believe that these peaks are due to intrinsic Ge impurities that are present in small amounts even in undoped commercial optical fibers [28]. However, it worth noticing that Si-ODCs and Ge-ODCs have almost overlapped emission spectra and comparable oscillation strength [25]. Therefore, UL between 400 and 500 nm in the step-index fiber may also have a contribution from Si-associated defects.

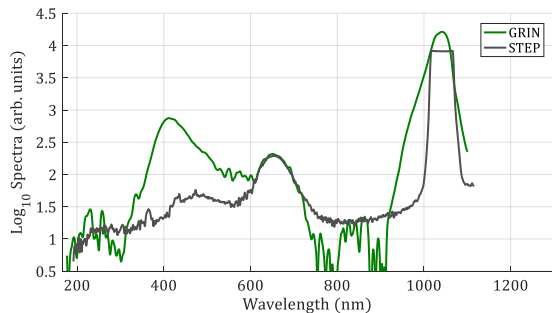


FIG. 6. Comparison of UL side-scattered spectra from either GRIN or step-index fibers, when the input peak power at 1030 nm is 2.2 MW. Curves plotted in \log_{10} scale are normalized to the same intensity value at 650 nm.

IV. CONCLUSION

In conclusion, we reported the observation of MPA excited UL in commercial multimode optical fibers. Based on our measurements, we estimate that MPA involving an average number of up to $n = 5$ photons is at the origin of the observed UL, in agreement with the expected position of the absorption bands. We could also directly relate the observed variation of side-scattered UL light intensity in GRIN fibers with simulated variation of MPA strength along the fiber. In perspective, UL can be exploited for extending the bandwidth of supercontinuum generation into UV frequencies. Moreover, the appearance of UL provides a useful tool to directly monitor the presence of nonlinear losses, at peak powers close to the damage threshold of optical fibers. Our results will be of importance across the range of widespread scientific and technological applications of optical fibers, for example in high-power fiber lasers, that will provide the next generation of particle accelerators, in nonlinear multiphoton microscopy and endoscopy, in laser ablation and micro machining, to name a few.

ACKNOWLEDGMENTS

We acknowledge support from the European Research Council (ERC) under the European Union's Horizon 2020 research and innovation program (grant No. 740355 and grant No. 874596) and the Russian Ministry of Science and Education Grant No. 14.Y26.31.0017. The authors declare no conflicts of interest.

-
- [1] F. Varsanyi and G. H. Dieke, Ion-pair resonance mechanism of energy transfer in rare earth crystal fluorescence, *Phys. Rev. Lett.* **7**, 442 (1961).
- [2] M.-K. Tsang, G. Bai, and J. Hao, Stimuli responsive up-conversion luminescence nanomaterials and films for various applications, *Chem. Soc. Rev.* **44**, 1585 (2015).
- [3] J. Yao, C. Huang, C. Liu, and M. Yang, Upconversion luminescence nanomaterials: A versatile platform for imaging, sensing, and therapy, *Talanta* **208**, 120157 (2020).
- [4] S. A. Pollack, D. B. Chang, and N. L. Moise, Upconversion-pumped infrared erbium laser, *Journal of Applied Physics* **60**, 4077 (1986).
- [5] L. F. Johnson and H. J. Guggenheim, Infrared-pumped visible laser, *Applied Physics Letters* **19**, 44 (1971).
- [6] H. You and M. Nogami, Three-photon-excited fluorescence of $Al_2O_3 - SiO_2$ glass containing Eu^{3+} ions by femtosecond laser irradiation, *Applied Physics Letters* **84**, 2076 (2004).
- [7] H. You, T. Hayakawa, and M. Nogami, Upconversion luminescence of $Al_2O_3 - SiO_2 : Ce^{3+}$ glass by femtosecond laser irradiation, *Applied Physics Letters* **85**, 3432 (2004).
- [8] X. Meng, K. Tanaka, S. Murai, K. Fujita, K. Miura, and K. Hirao, Two-photon-excited fluorescence from silicate glass containing tantalum ions pumped by a near-infrared femtosecond pulsed laser, *Opt. Lett.* **31**, 2867 (2006).
- [9] P. G. Kazansky, H. Inouye, T. Mitsuyu, K. Miura, J. Qiu, K. Hirao, and F. Starrost, Anomalous anisotropic light scattering in ge-doped silica glass, *Phys. Rev. Lett.* **82**, 2199 (1999).
- [10] L. Skuja, The origin of the intrinsic 1.9 eV luminescence band in glassy SiO_2 , *Journal of Non-Crystalline Solids* **179**, 51 (1994).
- [11] L. Skuja, Optically active oxygen-deficiency-related centers in amorphous silicon dioxide, *Journal of Non-Crystalline Solids* **239**, 16 (1998).
- [12] M. Cannas and F. Messina, Bleaching of optical activity induced by uv laser exposure in natural silica, *Journal of Non-Crystalline Solids* **345-346**, 433 (2004).
- [13] F. Messina, F. Comand'e, and M. Cannas, Effects induced by 4.7 eV uv laser irradiation on pure silica core multimode optical fibers investigated by in situ optical absorption measurements, *Journal of Non-Crystalline Solids* **357**, 1985 (2011).
- [14] M. Kristensen, Ultraviolet-light-induced processes in germanium-doped silica, *Phys. Rev. B* **64**, 144201 (2001).
- [15] M. Gallagher and U. Osterberg, Time resolved 3.10 eV luminescence in germanium-doped silica glass, *Applied Physics Letters* **63**, 2987 (1993).
- [16] C. Hnatovsky, D. Grobncic, and S. J. Mihailov, Nonlinear photoluminescence imaging applied to femtosecond laser manufacturing of fiber bragg gratings, *Opt. Express* **25**, 14247 (2017).
- [17] D. Kudarauskas, G. Tamosauskas, M. Vengris, and A. Dubietis, Filament-induced luminescence and supercontinuum generation in undoped, yb-doped, and nddoped yag crystals, *Applied Physics Letters* **112**, 041103 (2018).
- [18] K. Krupa, A. Tonello, A. Barthélémy, T. Mansuryan, V. Couderc, G. Millot, P. Grelu, D. Modotto, S. A. Babin, and S. Wabnitz, Multimode nonlinear fiber optics, a spatiotemporal avenue, *APL Photonics* **4**, 110901 (2019).
- [19] L. G. Wright, S. Wabnitz, D. N. Christodoulides, and F. W. Wise, Ultrabroadband dispersive radiation by spatiotemporal oscillation of multimode waves, *Phys. Rev. Lett.* **115**, 223902 (2015).
- [20] L. G. Wright, D. N. Christodoulides, and F. W. Wise, Controllable spatiotemporal nonlinear effects in multimode fibres, *Nature Photon* **9** 306-310 (2015).
- [21] M. Zitelli, F. Mangini, M. Ferraro, A. Niang, D. Kharenko, and S. Wabnitz, High-energy soliton fission dynamics in multimode grin fiber, *Opt. Express* **28**, 20473 (2020).
- [22] T. Hansson, A. Tonello, T. Mansuryan, F. Mangini, M. Zitelli, M. Ferraro, A. Niang, R. Crescenzi, S. Wabnitz, and V. Couderc, Nonlinear beam self-imaging and self-focusing dynamics in a grin multimode optical fiber: theory and experiments, *Opt. Express* **28**, 24005 (2020).
- [23] L. G. Wright, D. N. Christodoulides, and F. W. Wise, Spatiotemporal mode-locking in multimode fiber lasers, *Science* **358**, 94 (2017).
- [24] M. Leone, S. Agnello, R. Boscaino, M. Cannas, and F. M. Gelardi, Conformational disorder in vitreous systems probed by photoluminescence activity in SiO_2 , *Phys. Rev. B* **60**, 11475 (1999).
- [25] S. Girard, A. Alessi, N. Richard, L. Martin-Samos, V. De Michele, L. Giacomazzi, S. Agnello, D. D. Francesca, A. Morana, B. Winkler, I. Reghioua, P. Paillet, M. Cannas, T. Robin, A. Boukenter, and Y. Ouerdane, Overview of radiation induced point defects in silica-based optical fibers, *Reviews in Physics* **4**, 100032 (2019).
- [26] M. Pollnau, D. R. Gamelin, S. R. Lüthi, H. U. Güdel, and M. P. Hehlen, Power dependence of upconversion luminescence in lanthanide and transition-metal-ion systems, *Phys. Rev. B* **61**, 3337 (2000).
- [27] M. Karlsson, D. Anderson, and M. Desaix, Dynamics of self-focusing and self-phase modulation in a parabolic index optical fiber, *Opt. Lett.* **17**, 22 (1992).
- [28] F. Messina, M. Cannas, and R. Boscaino, Generation of defects in amorphous SiO_2 assisted by two-step absorption on impurity sites, *Journal of Physics: Condensed Matter* **20**, 275210 (2008).